buildings

MDPI

Article

Analytical Study on the Random Seismic Responses of an Asymmetrical Suspension Structure

Min Chen [1], Xiongjie Liang [1], Zongwang Yang [1], Xinguang Ge [2,*] and Changchun Xu [3]

[1] China Construction Science and Industry Corotational Ltd., Shenzhen 518000, China
[2] School of Civil Engineering and Architecture, Liuzhou Institute of Technology, Liuzhou 545004, China
[3] Guangxi Hualan Engineering Management Co., Ltd., Nanning 530012, China
* Correspondence: xinguangge@outlook.com

Abstract: An asymmetrical suspension structure, without vertical column support and without supplying the flexibility of spatial arrangement, is more sensitive to ground movement. The structural responses of an asymmetrical suspension structure subjected to Clough–Penzien spectrum excitation were analytically investigated in this study. First, the governing equation was decoupled into an independent state equation in generalized coordinates through the real mode decomposition method and by creatively combining it with finite element methods to acquire modal coefficients. Through the pseudo excitation method (PEM), the frequent domain solution of the dynamic response was acquired, and its power spectrum density function was then quadratically decomposed to obtain its corresponding 0–2-order spectral moments. A practical case study was performed to verify the high accuracy and computational efficiency of the proposed closed-form solution comparative to the traditional PEM. Finally, an extended analysis of the effect of the suspended span and comparisons to a normal framed structure and symmetrical suspension structures were carried out. The analysis results indicate that the larger suspended span could consume more seismic energy and result in smaller horizontal displacement and acceleration. Moreover, the comparison results also point out that the existence of the suspension part showed better seismic energy dissipation capacity compared to the normal framed structure, and two symmetrical suspension parts also performed better than a single asymmetrical part in seismic energy dissipation.

Keywords: asymmetrical suspension structure; spectral moments; random seismic excitation; quadratic decomposition method

check for updates

Citation: Chen, M.; Liang, X.; Yang, Z.; Ge, X.; Xu, C. Analytical Study on the Random Seismic Responses of an Asymmetrical Suspension Structure. *Buildings* **2023**, *13*, 1435. https://doi.org/10.3390/buildings13061435

Academic Editor: Alberto Maria Avossa

Received: 24 March 2023
Revised: 27 April 2023
Accepted: 29 May 2023
Published: 31 May 2023

Copyright: © 2023 by the authors. Licensee MDPI, Basel, Switzerland. This article is an open access article distributed under the terms and conditions of the Creative Commons Attribution (CC BY) license (https://creativecommons.org/licenses/by/4.0/).

1. Introduction

A suspension structure, as a typical tree structural system [1,2], presented in Figure 1, is composed of three parts: the center core frame, the transversal truss carrying the suspended parts, and the suspended floors connected with trusses through rigid booms or wire rope. The vertical load of the suspended parts is transferred to the main structure by means of a special connection system, which results in prospective seismic performance subjected to ground motion [3,4]. Therefore, the strong artistic expression in architecture, flexibility in structural arrangement, rationality in load path, and high utilization of building materials can all be observed in suspension structure systems. Recently, this novel structural system has been widely used in libraries, stadiums, convention centers, and other public buildings, such as Marquette Plaza (formerly the Federal Reserve Bank of Minneapolis) in the USA and Guiyang International Conference and Exhibition Centre and Guangdong Museum in China.

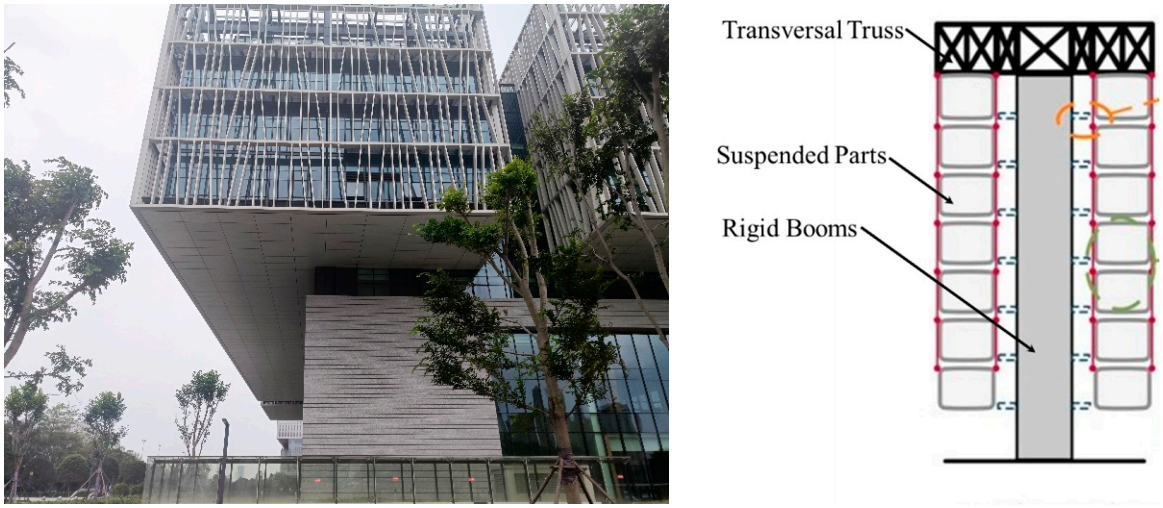


Figure 1. Picture and schematic of suspended structure. (**a**) Picture. (**b**) Schematic model [2].

Considering the mechanical performance of suspension structures, a theoretical analysis of a suspended roof under vertical static load was applied by Shimanovsky et al. [5] with the help of the three-dimensional elastic theory and the finite element method (FEM). Liu et al. [6] proposed a passive control system for suspension buildings with three performance levels based on stability and P-δ effect analysis. Combined with the characteristics of suspension structures, the structural vibration was reduced with the arrangement of rocking walls and connection damping. A novel CSI vibration isolation system, made of double-layer inclined rubber bearings and installed on top of the core frame, was also proposed by Saruta et al. [7], and its good seismic performance was confirmed by shaking table tests and long-term structural health monitoring [8]. The seismic responses of suspension buildings with viscous dampers under 20 ground motion time–history curves were analyzed in previous research [9], and the results indicated that the structural response was affected by the arrangement of dampers and the inter-layer stiffness. Moreover, Lv et al. [10] carried out an experimental study to discuss the crowd-activated vibration of suspended floors, and some suggestions for comfort design were obtained. The design parameter optimization of suspension parts in the vertical direction was carried out by Ye et al. [2] using a genetic algorithm. Optimal seismic parameter arrangement was obtained by maximizing the mean square moment of the main structures. The seismic response discussed in the abovementioned studies mainly focuses on buildings with symmetric suspension parts. However, one-sided suspension is also widely used in practice to obtain merits in architectural aesthetics and flexible space. Both horizontal and vertical movement, which have not been considered in previous research, would be stimulated with horizontal excitation in this kind of asymmetric suspension structure. Research on the horizontal–vertical coupled structural response of asymmetric suspension structures under random ground motion is important for practical engineering.

It has been revealed In many studies that randomness is noteworthy in ground motion and can be described by the power spectral density function in design [11–15]. With an extensive comparative study, an excitation model for random ground motion was proposed by Kanai et al. [16] and Tajimi et al. [17] to characterize the filtering of white noise. Although this random ground motion model, which considers the mechanical properties of soil, was widely accepted [18,19], some defects have also been pointed out [20]. To better describe the randomness in ground motion, a double-filtered white noise excitation model [21,22] with complex expressions was proposed to meet the needs of more scenarios. Cao et al. [23,24] carried out outstanding works on a consistent seismic hazard and fragility framework and an assessment on probabilistic seismic fragility analysis by comparing various probabilistic seismic fragility analyses. Regarding the methods of seismic response analysis,

time-domain and frequency-domain methods based on the random vibration theory are usually used [25,26]. The relationship between the double integrals of the covariance of structural response, the covariance of ground motion, and the structural impulse function is established using the time-domain method. The close-form solution of structural response is easy to obtain in this approach when the excitation belongs to white noise, while the solution would be verbose if the complex random seismic excitation was applied [27]. In the frequency-domain method, the concise relationship among the power spectral density function of structural response, the power spectral density function of ground motion excitation, and the frequency response function is established [28,29]. Still, numerical integration is required when analyzing the random characteristic value of the structural response, which leads to the limitation of calculation accuracy and efficiency [30]. The method decoupling power spectral density function of structural response has attempted to overcome the difficulties of complex seismic excitation models to achieve a closed-form solution [27,31]. However, the previous studies are limited to regular simple structures.

Gaining attention recently, the dynamic characteristics of suspension structures need to be fully studied and discussed. Research on their structural responses under random ground motion is still relatively scarce, and it is necessary to obtain theoretical analysis results to provide sufficient confidence for their application. The aim of this paper is to obtain the seismic responses of an asymmetrical suspension structure under the Clough–Penzien spectrum and to discuss the influences of design parameters on its dynamic characteristics. These may differ from common structures due to the special connection system in suspension structures, which brings challenges to the design process. In order to provide meaningful and practical suggestions, a practical asymmetrical suspension structure was studied in three steps. First, the dynamic equations governing the structural behaviors were established. To obtain the necessary modal parameters in the equations, a finite element model of the studied structure was used for modal analysis. The complex governing dynamic equation was decoupled through the real model method, and its basic mode coefficients and frequency-domain solutions of decoupled independent variables were subsequently solved by the pseudo excitation method (PEM). Then, the equations were solved in the second step. The quadratic decomposition of the PSDF of structural responses and deduction of its closed-form solution are presented, as well as verification of its accuracy and computational efficiency. In the third step, comparative studies were applied by adjusting numerical models and their corresponding modal parameters. With the aspect of both horizontal and vertical displacement and acceleration, the effects of suspended span and symmetry are discussed.

2. Seismic Response of an Asymmetrical Suspension Structure

2.1. Seismic Equation in Generalized Coordinates

An asymmetrical suspension structure, composed of three main parts: a vertical support part, a horizontal cantilever part, and a vertical suspension part, which is asymmetrically distributed, is conceptually represented in Figure 2. The vertical support part usually adopts a framed structure system or a shear wall system, which relies on the height of the building. The horizontal cantilever part is composed of a suspender and truss cantilever beam system. The suspension part is located below the cantilever beam and is suspended without vertical column support.

When subjected to earthquake excitation, the basic motion equation of the asymmetrical suspension structure can be expressed as:

$$\boldsymbol{M}\ddot{\boldsymbol{x}} + \boldsymbol{C}\dot{\boldsymbol{x}} + \boldsymbol{K}\boldsymbol{x} = \boldsymbol{M}\boldsymbol{I}\ddot{x}_g(t) \quad (1)$$

where $\ddot{\boldsymbol{x}}$, $\dot{\boldsymbol{x}}$, $\boldsymbol{x}$ are the horizontal and vertical acceleration, velocity, and displacement vectors of the structure nodes relative to the ground, respectively, which all are $n \times 1$-order vectors. n is the total freedom of the suspension structure with consideration of bidirectional vibration. $\boldsymbol{M}$, $\boldsymbol{K}$, $\boldsymbol{C}$ are the mass, stiffness, and damping matrices of the structure, respectively, which are all the n-order square matrix. $\boldsymbol{I}$ is the position parameter of the horizontal ground motion, whose values are equal to 1 for structural horizontal freedoms and equal to 0 for structural vertical freedoms. $\ddot{x}_g(t)$ is the absolute acceleration of ground horizontal movement in the field caused by seismic excitation.

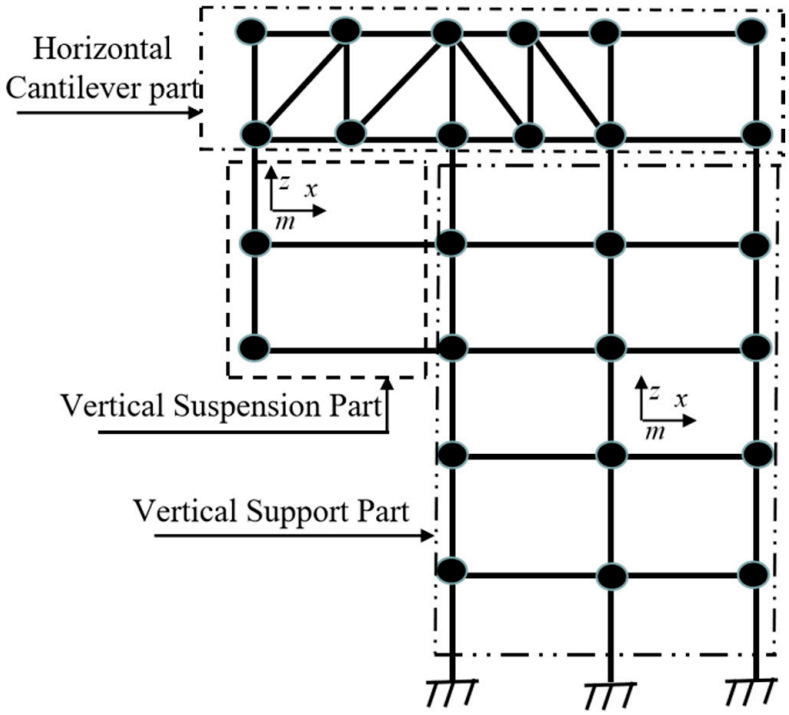


Figure 2. Conceptual schematic of the asymmetric suspension structure.

Due to the vibration complexity of asymmetrical suspension structures and its multiple freedoms, it is not possible to solve asymmetrical suspension structure seismic responses directly from Equation (1) because the basic seismic equation is coupled. Thus, the real model method was then applied to decouple the basic seismic equation and translate it into the linear combination of an independent dynamic equation of oscillators in generalized coordinates.

As for the real mode transformation, numerical modeling was applied in this study to obtain the corresponding coefficients, including the concentrate mass matrix, the natural frequency matrix, and the mode shape of the asymmetrical suspension structure. It is relatively easy to obtain the basic dynamic coefficients of an asymmetrical suspension structure based on numerical modeling in most commercial finite element software. According to the real mode method, by introducing generalized variable q, the node displacement vector $\boldsymbol{x}$ can be represented as Equation (2), when only former N-modes shapes are considered.

$$\boldsymbol{x} = \phi\boldsymbol{q} \quad (2)$$

where ϕ represents former N-modes of the asymmetrical suspension structure, and it is an $n \times N$-order matrix.

Substituting Equation (2) into Equation (1), the basic seismic equation is decoupled into Equation (3) with the generalized coordinate as the variable.

$$\ddot{\boldsymbol{q}} + 2\xi\boldsymbol{\omega}\dot{\boldsymbol{q}} + \boldsymbol{\omega}^2\boldsymbol{q} = \boldsymbol{\alpha}\ddot{x}_g(t) \tag{3}$$

where $\boldsymbol{q} = \{q_1, \ldots, q_N\}^{\mathrm{T}}$, $\boldsymbol{\omega}$ denotes the natural frequency matrix of the asymmetrical suspension structure, and $\boldsymbol{\omega} = \mathrm{diag}(\omega_1, \ldots, \omega_N)$. ξ denotes the damping ratio. $\boldsymbol{\alpha} = \left(\phi^{\mathrm{T}}\boldsymbol{M}\phi\right)^{-1}\phi^{\mathrm{T}}\boldsymbol{M}\boldsymbol{I}$.

2.2. Frequency-Domain Solution of Seismic Responses

Equation (3) is a second-order differential equation, and the complex mode method (CMM) is employed to reduce its differential order for the convenience of obtaining a frequency-domain solution. The state variable in the form of a column vector is first introduced as:

$$\boldsymbol{y} = \begin{Bmatrix} \boldsymbol{q} \\ \dot{\boldsymbol{q}} \end{Bmatrix} \tag{4}$$

According to the CMM and by combining Equation (4) with Equation (3), the second-order differential seismic equation can be translated into Equation (5), which then shows in a one-order differential form:

$$\overline{\boldsymbol{M}}\dot{\boldsymbol{y}} + \overline{\boldsymbol{K}}\boldsymbol{y} = \boldsymbol{r}\ddot{x}_g(t) \tag{5}$$

where $\widehat{\boldsymbol{M}} = \begin{bmatrix} E & \boldsymbol{o}_1 \\ \boldsymbol{o}_1 & E \end{bmatrix}$, $\widehat{\boldsymbol{K}} = \begin{bmatrix} \boldsymbol{o}_1 & -\boldsymbol{E} \\ \boldsymbol{\omega}^2 & 2\xi\boldsymbol{\omega} \end{bmatrix}\boldsymbol{r} = -\begin{bmatrix} \boldsymbol{o}_2 \\ \boldsymbol{\alpha} \end{bmatrix}$, $\boldsymbol{E}$ is an $\boldsymbol{N}$-order unit diagonal matrix, $\boldsymbol{o}_1$ is the $\boldsymbol{N}$-order square matrix, and $\boldsymbol{o}_2$ is the $\boldsymbol{N}\square 1$-order vector.

Based on the CMM, there must be right and left eigenvectors $\boldsymbol{V}$ and $\boldsymbol{U}$, as well as eigenvalue matrix $\boldsymbol{P}$ for Equation (5), which can satisfy the complex mode decoupling. When applying complex transformation $\boldsymbol{y} = \boldsymbol{U}\boldsymbol{z}$, Equation (5) is transferred into an orthogonalized matrix form with the independent variable of z:

$$\dot{\boldsymbol{z}} + \boldsymbol{P}\boldsymbol{z} = \boldsymbol{\eta}\ddot{x}_g(t) \tag{6}$$

where $\boldsymbol{\eta} = \frac{\boldsymbol{V}^T\boldsymbol{r}}{\boldsymbol{V}^T\overline{\boldsymbol{M}}\boldsymbol{U}}$ and it is a $2N\square 1$-order column vector.

It is known that $\boldsymbol{P}$ is a diagonal matrix; combining its expression, Equation (6) can be regarded as the linear combination of $2N$ dependent components. Therefore, its components equation can be expressed as:

$$\dot{z}_i + p_i z_i = \eta_i \ddot{x}_g(t) \quad (i = 1 \sim 2N) \tag{7}$$

where z_i, η_i, p_i are the ith components of $\boldsymbol{z}$, $\boldsymbol{\eta}$, $\boldsymbol{P}$, respectively.

The frequency-domain solution of Equation (7) can be solved by the pseudo excitation method (PEM) directly. Thus, the frequency-domain solution of component $z_i(\omega)$ is given as below:

$$z_i(\omega) = \frac{\eta_i\sqrt{S_{\ddot{x}_g}(\omega)}e^{\mathrm{j}\omega t}}{\mathrm{j}\omega + p_i} \quad (i = 1 \sim 2N) \tag{8}$$

where $S_{\ddot{x}_g}(\omega)$ is the power spectrum density function of seismic excitation $\ddot{x}_g(t)$. In this study, the Clough–Penzien spectrum was employed as the random seismic excitation.

The Clough–Penzien spectrum has been widely applied in engineering because it treats the ground soil as two associated linear filters and overcomes the shortcoming of overstating the low-frequency energy of Kanai–Tajimi. Based on earlier reports, the power spectrum density function of the Clough–Penzien spectrum can be expressed as:

$$S_{\ddot{x}_g}(\omega) = \frac{\omega^4}{\left(\omega_f^2 - \omega^2\right)^2 + 4\xi_f^2\omega_f^2\omega^2} \frac{\omega_g^4 + 4\xi_g^2\omega_g^2\omega^2}{\left(\omega_g^2 - \omega^2\right)^2 + 4\xi_g^2\omega_g^2\omega^2} S_0 \tag{9}$$

where $\xi_f, \xi_g, \omega_f, \omega_g$ are the vibration characteristic values of the ground soil, and S_0 is the seismic intensity coefficient.

Equation (8) gives the frequency-domain solution of complex mode variable z. In addition, the frequency-domain solution of the generalized variable can be obtained from the equation of the complex mode variable and the state variable (i.e., $\boldsymbol{y} = \boldsymbol{U}\boldsymbol{z}$) and the relationship between the state variable and the generalized variable (i.e., Equation (4)). Consequently, the frequency-domain solutions of the generalized variable and its first-order differential are solved as below:

$$\begin{aligned} q_k(\omega) &= \sum_{i=1}^{2N} u_{k,i} z_i(\omega) \\ \dot{q}_k(\omega) &= \sum_{i=1}^{2N} u_{k+N,i} z_i(\omega) \end{aligned} \tag{10}$$

Similarly, considering the relationship between the generalized variable and the nodal displacement and replacing Equation (2) into Equation (10), the frequency-domain solution of nodal displacement x_k and nodal velocity $\dot{x}_k$ can be obtained as follows:

$$\begin{aligned} x_k(\omega) &= \sum_{l=1}^{N} \sum_{i=1}^{2N} \phi_{k,l} u_{l,i} z_i(\omega) = \sum_{i=1}^{2N} \widetilde{\lambda}_{k,i} z_i(\omega) \\ \dot{x}_k(\omega) &= \sum_{l=1}^{N} \phi_{k,l} u_{N+l,i} \sum_{i=1}^{2N} z_i(\omega) = \sum_{i=1}^{2N} \overline{\lambda}_{k,l} z_i(\omega) \end{aligned} \tag{11}$$

where $\phi_{k,l}$ is the (k, l) element of asymmetrical suspension structure mode shape $\boldsymbol{\phi}$, and $u_{l,i}$ is the corresponding (k, l) element of the right eigenvector $\boldsymbol{U}$. $\widetilde{\lambda}_{k,i} = \sum_{l=1}^{N} \phi_{k,l} u_{l,i}$ and $\overline{\lambda}_{k,l} = \sum_{l=1}^{N} \phi_{k,l} u_{N+l,i}$, and they are response model intensity coefficients.

Through analyzing the expression form of the frequency-domain solution of the generalized variable and its gradient, nodal displacement, and nodal velocity, it can be seen that they are all in a similar formation. Thus, they are unified into the solution of generalized response X, as Equation (12):

$$X(\omega) = \sum_{i=1}^{2N} \gamma_i z_i(\omega) \tag{12}$$

where γ_i is ith mode intensity coefficient of response X.

3. Closed-Form Solution of Seismic Response Spectrum Moments

3.1. Quadratic Decomposition of the PSDF of Dynamic Responses

Based on the PEM, the PSDF of the structural response can be expressed by the multiplication of its frequency-domain solution and the corresponding complex conjugate term as Equation (13):

$$S_X(\omega) = X(\omega) \times X^*(\omega) = \sum_{k=1}^{2N} \sum_{i=1}^{2N} \gamma_k \gamma_i z_k(\omega) z_i^*(\omega) \tag{13}$$

where $X^*(\omega)$ is the complex conjugate term of $X(\omega)$; thus, $X^*(\omega) = X(-\omega)$. Similarly, $z_i^*(\omega)$ is the complex conjugate term of $z_i(\omega)$ and $z_i^*(\omega) = z_i(-\omega)$.

Substituting the expression of the frequency-domain solution of complex mode $z_i(\omega)$, i.e., Equation (8), into Equation (13), the PSDF of the structural response can be expressed as:

$$S_X(\omega) = \sum_{k=1}^{2N}\sum_{i=1}^{2N}\gamma_k\gamma_i\frac{\eta_i\sqrt{S_{\ddot{x}_g}(\omega)}e^{-\mathrm{j}\omega t}}{-\mathrm{j}\omega + p_i}\frac{\eta_k\sqrt{S_{\ddot{x}_g}(\omega)}e^{\mathrm{j}\omega t}}{\mathrm{j}\omega + p_k} = S_{\ddot{x}_g}(\omega)H_X(\omega) \tag{14}$$

where

$$H_X(\omega) = \sum_{k=1}^{2N}\sum_{i=1}^{2N}\frac{\rho_i}{\mathrm{j}\omega + p_i}\frac{\rho_k}{\mathrm{j}\omega + p_k} \tag{15}$$

where $\rho_w = k_w\eta_w (w = i, k)$.

The spectral moment is used to measure the magnitude of the structural dynamic response under random excitation. It is the integral of the response to the PSDF on the interval $[-\infty, +\infty]$. Due the complex form of $S_{\ddot{x}_g}(\omega)$ and $H_X(\omega)$ in Equation (14), it is difficult to obtain the analytical solution and the integral solution directly.

By analyzing the form of $H_X(\omega)$, taking the rational decomposition of Equation (15), it can be converted into:

$$H_X(\omega) = \sum_{i=1}^{2N}\frac{{\rho_i}^2}{\omega^2 + p_i^2} + 2\sum_{k=1}^{2N-1}\sum_{i=k+1}^{2N}\frac{\rho_i\rho_k}{p_i + p_k}\left(\frac{p_i}{\omega^2 + p_i^2} + \frac{p_k}{\omega^2 + p_k^2}\right) \tag{16}$$

Similarly, based on the residue theorem, the PSDF of the Clough–Penzien spectrum, i.e., Equation (9), can be quadratically decomposed as below:

$$S_{\ddot{x}_g}(\omega) = S_0\sum_{m=1}^{2}\sum_{n=1}^{2}\left(1 - \frac{c_{f,n}}{\omega^2 + \omega_{f,n}^2}\right)\frac{c_{g,m}}{(\omega^2 + \omega_{g,m}^2)} \tag{17}$$

where $\omega_{f,1}^2 = (2\xi_\mathrm{f}^2 - 1)\omega_\mathrm{f}^2 - 2\omega_\mathrm{f}^2\xi_\mathrm{f}\sqrt{\xi_\mathrm{f}^2 - 1}$, $\omega_{g,1}^2 = (2\xi_\mathrm{g}^2 - 1)\omega_\mathrm{g}^2 - 2\omega_\mathrm{g}^2\xi_\mathrm{g}\sqrt{\xi_\mathrm{g}^2 - 1}$, $c_{f,1} = \frac{\omega_f^4 + 2\times\omega_f^2\times\omega_{f,1}^2\times(1-2\times\xi_\mathrm{f}^2)}{\omega_{f,2}^2 - \omega_{f,1}^2}$, $c_{\mathrm{g},1} = \frac{\omega_\mathrm{g}^4 - 4\xi_\mathrm{g}^2\omega_\mathrm{g}^2\omega_{g,1}^2}{\omega_{g,2}^2 - \omega_{g,1}^2}$, $\omega_{f,2}^2 = \mathrm{conj}(\omega_{f,1}^2)$, $\omega_{g,2}^2 = \mathrm{conj}(\omega_{g,1}^2)$, $c_{f,2} = \mathrm{conj}(c_{f,1})$, and $c_{g,2} = \mathrm{conj}(c_{g,1})$.

Based on the integral criterion, through the quadratic form, it is possible to obtain the analytical and integral solution. After the quadratic decomposition of $S_{\ddot{x}_g}(\omega)$ and $H_X(\omega)$ as Equations (16) and (17) and then their substitution into Equation (14), the quadratic decomposition of the PSDF of the structural responses is given as follows:

$$S_X(\omega) = \sum_{i=1}^{2N}\rho_i^2 A_i(\omega) + 2\sum_{i=1}^{2N-1}\sum_{k=i+1}^{2n}\frac{\rho_k\rho_i}{p_k + p_i}[p_i A_i(\omega) + p_k A_k(\omega)] \tag{18}$$

where

$$A_i(\omega) = S_0\sum_{m=1}^{2}\sum_{n=1}^{2}\left(1 - \frac{c_{f,n}}{\omega^2 + \omega_{f,n}^2}\right)\frac{c_{g,m}}{(\omega^2 + \omega_{g,m}^2)}\frac{1}{p_i^2 + \omega^2} \tag{19}$$

3.2. Closed-Form Solution of 0–2-Order Spectrum Moments

It is known that the 0–2-order spectrum moments are necessary factors for Markov dynamic reliability analysis. According to the definition of spectrum moments, the q-order (q = 0, 1) spectrum moments of dynamic response $\alpha_{X,q}$ are given as Equation (20). As for the second-order spectrum moment, it can be obtained from the fundamental equivalence

relationship in the field of random vibration, i.e., the second-order spectrum moment is equal to the zero-order spectrum moment (the variance) of its rate of change.

$$\begin{gathered} \alpha_{X,q} = 2\int_0^\infty \omega^q S_X(\omega)\mathrm{d}\omega \quad (q = 0, 1) \\ \sigma_X^2 = \alpha_{X,0}, \sigma_{\dot{X}}^2 \\ \sigma_{\dot{X}}^2 = \alpha_{X,2} = \alpha_{\dot{X},0} \end{gathered} \tag{20}$$

where $\dot{X} = \frac{\mathrm{d}X}{\mathrm{d}t}$ and $\sigma_X^2, \sigma_{\dot{X}}^2$ are the variances of the dynamic response and its rate of change.

When substituting Equation (18) into Equation (20) and conducting the integration, we obtain the closed-form solution of the 0–1-order spectrum moments as Equation (21), because the integration of the product of ω^q (q = 0, 1) and the quadratic PSDF of the dynamic response has an analytical solution in [0, +∞].

$$\alpha_{X,s} = \sum_{i=1}^{2N} \rho_i^2 \chi_{i,s} + 2\sum_{i=1}^{2N-1}\sum_{k=i+1}^{2N} \frac{\rho_k \rho_i}{p_k + p_i}(p_i \chi_{i,s} + p_k \chi_{k,s}) \quad (s = 0, 1, 2) \tag{21}$$

where

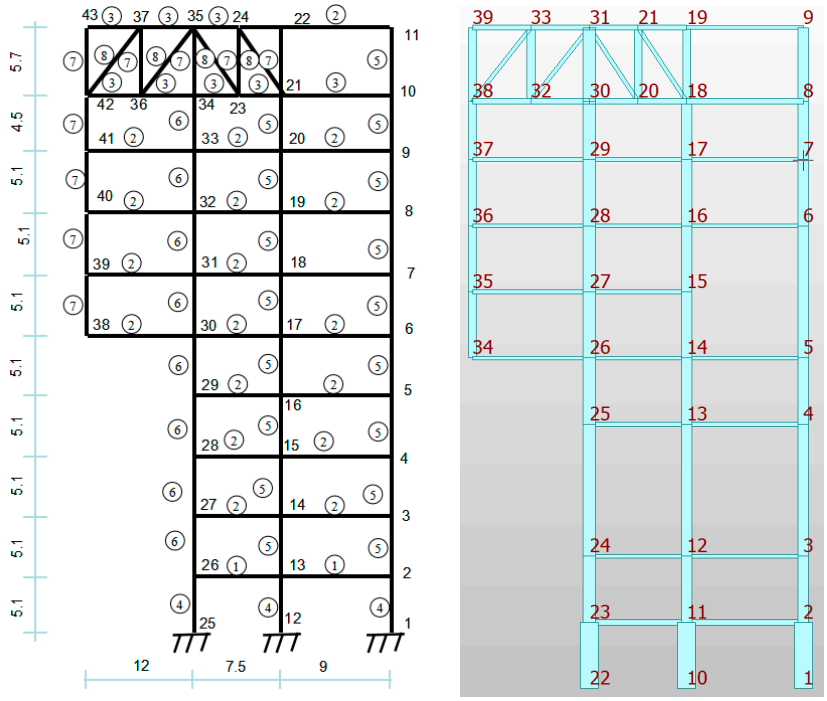
$$\begin{gathered} \chi_{i,s} = S_0 \sum_{m=1}^{2} c_{g,m}\sigma_{gmi,s} - S_0 \sum_{m=1}^{2}\sum_{n=1}^{2} \frac{c_{f,n}c_{g,p}}{\omega_{f,n}^2 - \omega_{g,p}^2}\left(\sigma_{fni,s} - \sigma_{gmi,s}\right) \quad s = 0, 1 \\ \chi_{i,2} = S_0\pi \sum_{m=1}^{2} \frac{c_{g,m}}{\omega_{g,m}} - S_0\pi \sum_{m=1}^{2}\sum_{n=1}^{2} c_{f,n}c_{g,m}\sigma_{gfmn,0} - p_i^2\chi_{i,0} \end{gathered} \tag{22}$$

where $\rho_{gmi,0} = \pi\left[\omega_{g,m}p_i(\omega_{g,m} + p_i)\right]^{-1}$, $\rho_{gm,1} = \frac{c_{g,m}}{p_i^2 - \omega_{g,m}^2}\left(\ln p_i^2 - \ln \omega_{g,m}^2\right)$, and $\rho_{gfnm,0} = \omega_{g,m}\omega_{f,n}\left(\omega_{g,m} + \omega_{f,n}\right)\pi$.

$\chi_{i,s}$ from Equation (22), it can be seen that $\chi_{i,s}$ is an analytical expression, and it is also easy to obtain the accurate numerical values of ρ_w and p_w from matrix computation. Therefore, it can be seen that the 0–2-order spectrum moments expressed in Equation (21) are a closed-form solution.

3.3. Closed-Form Solution Verification

A practice library program, for aesthetic effect, employs the asymmetrical suspension structure. The library comprises nine steel floors aboveground and one reinforced concrete floor underground. For simplification, a pin structure was taken as the example for seismic analysis in this study; its geometry message is presented in Figure 3a, and all of the geometry units are in meters. The node number and element type number are also shown in Figure 3a. The elements section characteristics are collected and listed in Table 1. For obtaining dynamic characteristic coefficients, the commercial software Midas Gen was applied to model the asymmetrical suspension library as shown in Figure 3b. There are 43 nodes and 8 kinds of element sections. Both the horizontal and vertical vibrations are considered, and 86 freedoms exist in this dynamic analysis. Nodal mass is regarded as the concentrated mass, comprising the structure self-weight, paving weight, and life load, whose calculations obey the dependent area method. In this study, the paving load was 1 kN/m^2, and the life load was 5 kN/m^2. The stiffness of the asymmetrical suspension structure was calculated based on the structural mechanics method. As for the damping ratio, the steel nodes were equal to 2%, the reinforced concrete nodes were equal to 5%, and the adjacent nodes were equal to the lower value. The ground site and motion coefficients were listed as: ω_g = 15.71 rad/s, ξ_g = 0.8, $\omega_f = 0.4\omega_g$, $\xi_f = \xi_g$, $S_0 = 1.11 \times 10^{-2}$ m^2/s^3.



(**a**) (**b**)

Figure 3. Schematic of the asymmetrical suspension library. (**a**) Nodes and elements distribution. (**b**) Finite element model.

Table 1. Element section characteristics.

Number	Materials	Section Characteristics (mm)
①	C30	Rectangular 650 × 400
②	Q390	H700 × 300 × 20 × 40
③	Q390	H1000 × 400 × 30 × 80
④	C35	Rectangular 1400 × 1400
⑤	Q390	Box 800 × 800 × 50
⑥	Q390	Box 1000 × 1000 × 80
⑦	Q390	Box 600 × 600 × 20
⑧	Q390	H600 × 300 × 30 × 90

The PEM is a commonly used method for engineering structure random dynamic analysis, which adopts numerical integration for spectrum moments calculation. Thus, the shortcomings are that the accuracy and efficiency of the spectrum moments calculated by the PEM are significantly affected by the integration range and integration interval. According to Equation (3), the frequency solution of the generalized variable through the PEM can be solved as:

$$q_i(\omega) = \frac{\alpha_i \sqrt{S_{\ddot{x}_g}(\omega)} e^{j\omega t}}{-\omega^2 + 2j\xi\omega_i + \omega_i^2} \tag{23}$$

Consequently, the PSDF of the structural dynamic response can be obtained as:

$$S_{x_i}(\omega) = x_i(\omega) \times x_i^*(\omega) = S_{\ddot{x}_g}(\omega) \sum_{l=1}^{N} \sum_{k=1}^{N} \frac{\phi_{ik}\alpha_k}{-\omega^2 - 2j\xi\omega_k + \omega_k^2} \frac{\phi_{il}\alpha_l}{-\omega^2 + 2j\xi\omega_l + \omega_l^2} \tag{24}$$

According to Equation (24), the calculation of structural response spectrum moments can only use numerical integration.

Taking the former 30-order modes into account, the 0–2-order spectrum moments of horizontal and vertical displacement were calculated using the proposed method and the PEM with various integration intervals. In addition, the comparison results were collected and are presented in Figures 4–9. The findings show that with a reduction in the integration interval, the spectrum moments estimated using the PEM tended to be stable. The numerical integration characteristics confirm that the integration results were more accurate with the reduction in the integration interval. Moreover, it can be seen that the stable results coincided with the results from the proposed method, and all of the results, including different spectrum moments of horizontal and vertical displacement, showed the same tendency. Thus, those results can verify and confirm the accuracy of the proposed method. Those cases were calculated using the same private PC, and the time–cost of the PEM with various intervals were collected as: 0.11 s for $\Delta\omega$ = 0.5 rad/s, 0.68 s for $\Delta\omega$ = 0.1 rad/s, and 6.30 s for $\Delta\omega$ = 0.5 rad/s. However, it only consumes 0.3 s for the proposed method. These results represent the high calculation efficiency of the proposed method. The high accuracy and efficiency of the proposed method are the main advantages of the proposed closed-form solution.

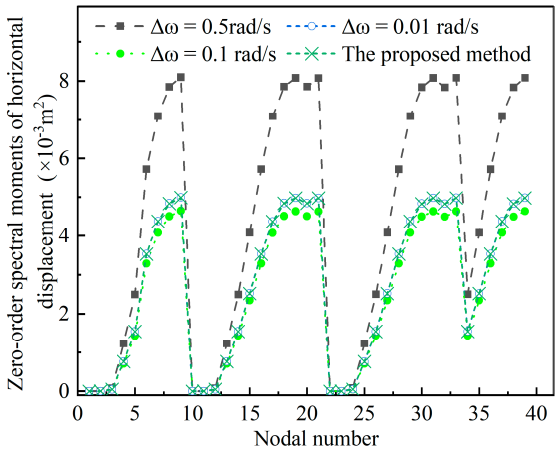


Figure 4. Zero-order spectral moments of horizontal node displacement.

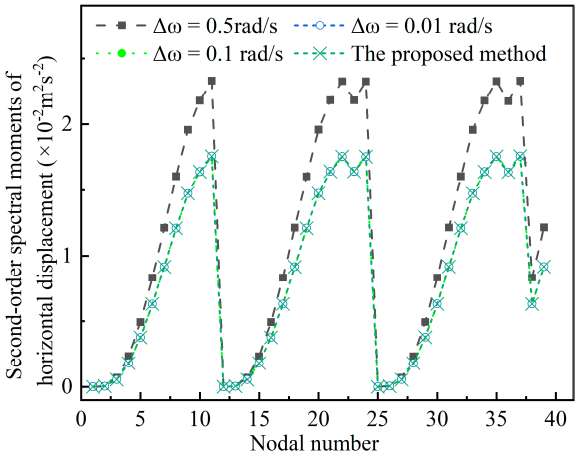


Figure 5. First-order spectral moments of horizontal node displacement.

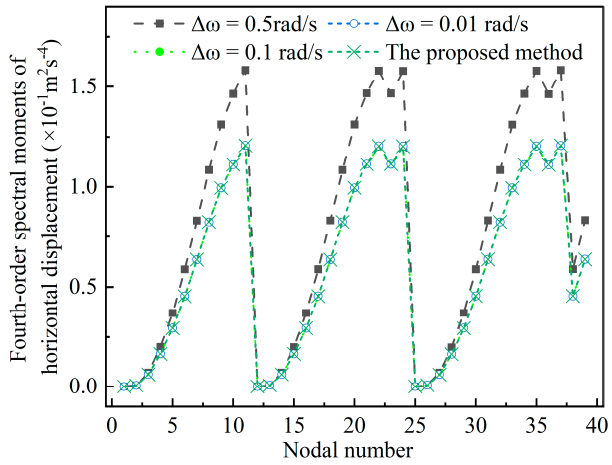


Figure 6. Second-order spectral moments of horizontal node displacement.

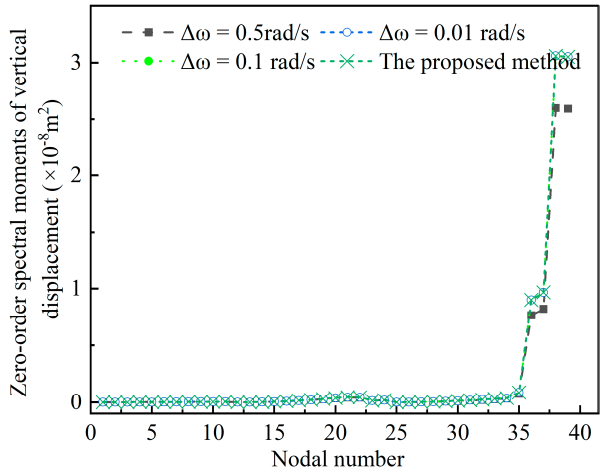


Figure 7. Zero-order spectral moments of vertical node displacement.

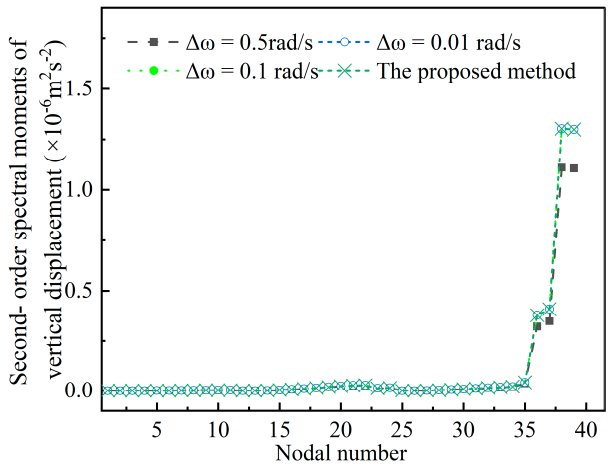


Figure 8. First-order spectral moments of vertical node displacement.

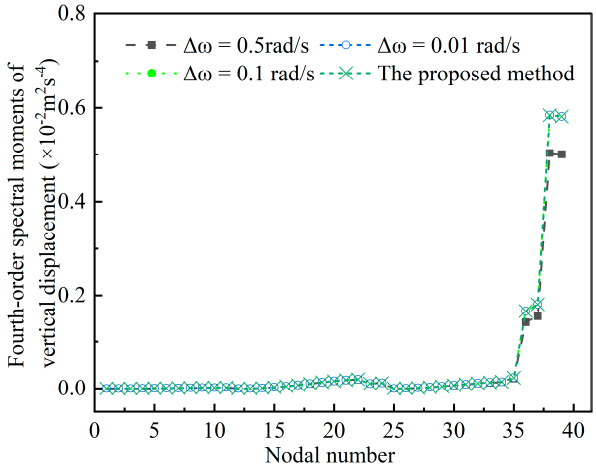


Figure 9. Second-order spectral moments of vertical node displacement.

4. Extended Comparison and Discussion

4.1. Effect of the Suspended Span

With the convenience of the proposed method to accurately and efficiently predict the dynamic responses of the asymmetrical suspended structure, the effect of the suspended span is studied in this section, which is the most significant factor in the asymmetrical suspended structure. Based on the practice asymmetrical suspended library, four suspended spans, including a span of 4.5 m, a span of 9 m, a span of 13.5 m, and a span of 18 m, were parametrically studied to explore the effect of span on horizontal and vertical responses under random horizontal seismic excitation (Clough–Penzien spectrum). The analysis process of solving the dynamic responses of suspension structures under seismic excitation followed the process of deduction of finite element model modeling and basic structural mode coefficients acquirement; dynamic governing equation establishment; and decoupling, solving, and quadratic decomposition of the PSDF of dynamic responses for its closed-form solution. The detailed equations and deductions are given in Sections 3 and 4, and all of the computations were performed using MATLAB programming.

Figure 10 presents the numerical model schematic of the asymmetrical suspended structure with various suspended spans. In this parametric study, the interval of the vertical element in the truss was 4.5 m. The span of 9 m was regarded as the reference model, and the nodes' numbering was also based on that reference model.

The comparison results of horizontal displacement and acceleration are illustrated in Figure 11. From Figure 11a, it can be seen that the horizontal displacement increased with the nodal height, and the horizontal displacement results were almost the same as the nodes of the same height, including the nodes in the suspended part, which demonstrates that the asymmetrical suspended structure also followed the assumption of plane stiffness infinite under horizontal seismic excitation. From Figure 11b, the horizontal accelerations varied with the increase in height. Among the various suspended spans, it is interesting that the asymmetrical suspended structure with the larger suspended span presented small horizontal displacement and acceleration, as presented in Figure 11a,b. The results were predominantly caused by the existing suspended part consuming the seismic energy through vertical vibration and the larger suspended span consuming more energy; this resulted in smaller horizontal displacement and acceleration. These results also confirm the previous reports [32–35] in that the suspended structure presented better horizontal anti-seismic behavior. The vertical response results of the asymmetrical suspended structure are presented in Figure 11c,d. It can be observed that the maximum vertical displacements (located at the suspended part, numbers 34–39) increased with the suspended span under horizontal seismic excitation, as shown in Figure 11c. Meanwhile, it can be observed that the vertical displacements of the asymmetrical suspended structures, except those with the suspended span of 18 m, were one magnitude smaller than the corresponding horizontal displacements, and their maximum

value was still smaller than 2 mm. However, the asymmetrical suspended structure with the suspended span of 18 m represented a booming vertical displacement (up to 10 mm) in the suspended part, which could cause structural damage, and this cannot be accepted in practical engineering. The vertical accelerations of various suspended spans did not show regularity in the increase in the span, as shown in Figure 11d. Moreover, the vertical accelerations in the suspended part could reach nearly half of the corresponding horizontal acceleration, except in the case with the measurement of 13.5 m, which shows that the vertical force caused by the horizontal seismic load cannot be ignored.

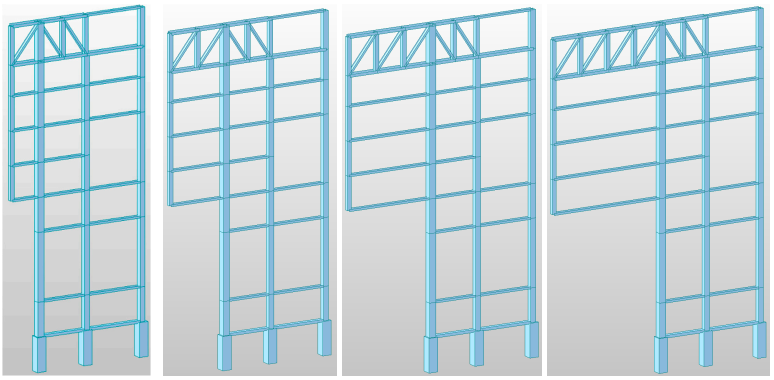


Figure 10. Schematic of the asymmetrical suspended structures with various suspended spans: (**a**) a span of 4.5 m; (**b**) a span of 9 m; (**c**) a span of 13.5 m; and (**d**) a span of 18 m.

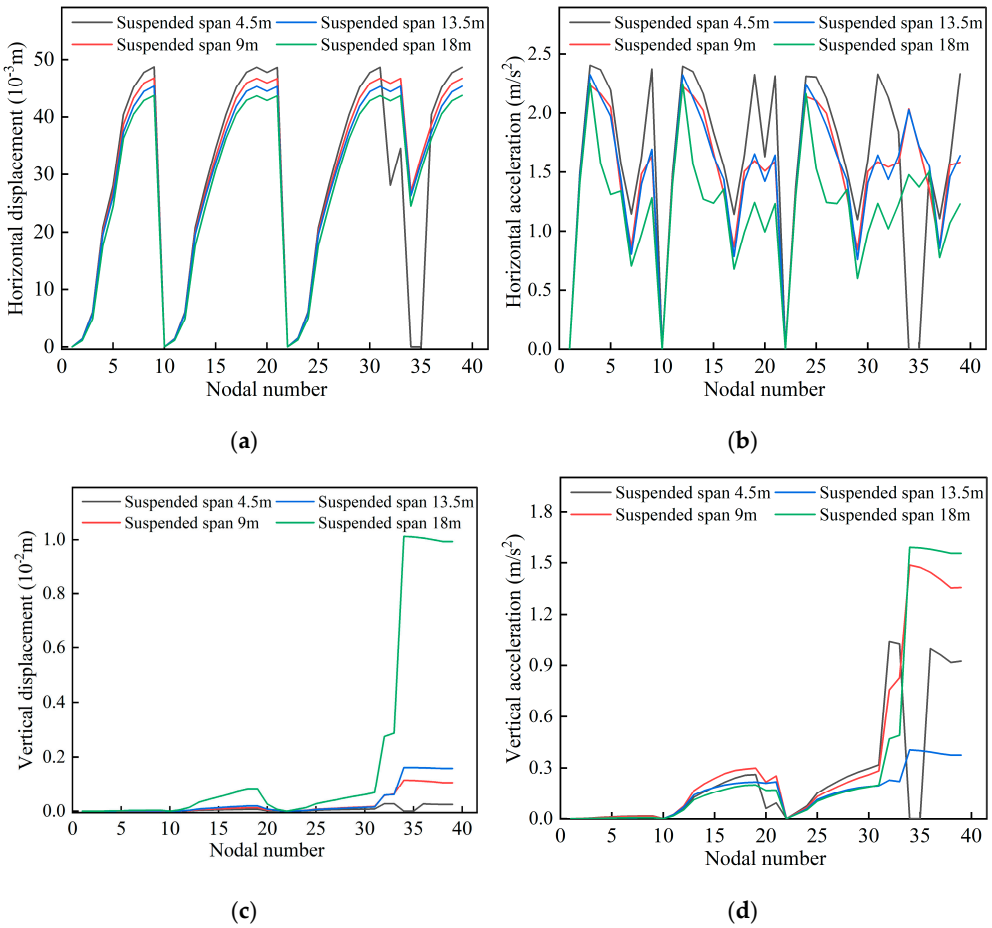


Figure 11. The effect of the suspended span on the horizontal responses. (**a**) Horizontal displacement. (**b**) Horizontal acceleration. (**c**) Vertical displacement. (**d**) Vertical acceleration.

4.2. Comparison to the Normal Framed Structure

A comparison of the seismic responses between the asymmetrical suspended structure and the normal framed structure is carried out in this section. The comparatively normal framed structure was based on the asymmetrical suspended structure mentioned in Section 3.3, and the columns were added below the suspended part. The schematic and structural arrangement of the normal framed structure are given in Figure 12a, and the section properties of the added columns are the same as their adjacent columns as shown in Figure 12b. The node numbering of the normal framed structure was based on the referred asymmetrical suspended structure, and the nodal numbers of added columns followed the maximum number of the referenced asymmetrical suspended structure as shown in Figure 12b.

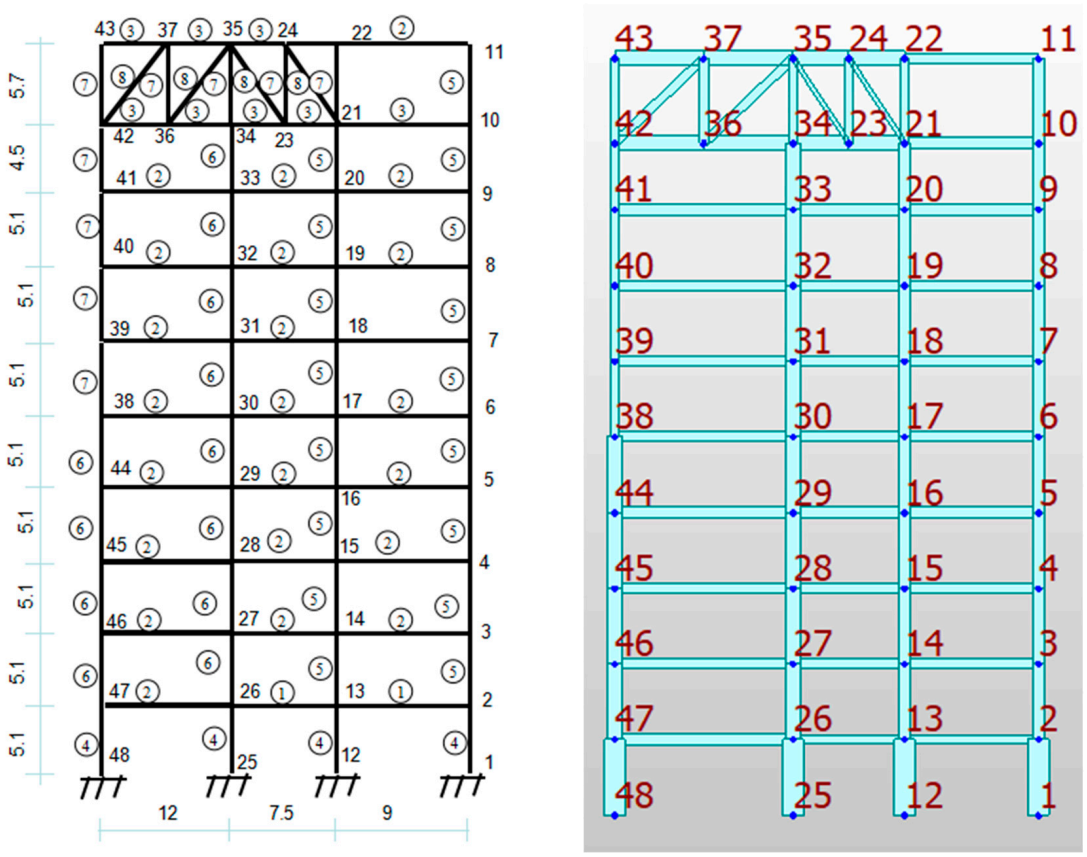


Figure 12. Schematic of the normal framed structure. (**a**) Normal framed structure arrangement. (**b**) Finite element model.

Figure 13 presents the comparison results of the seismic responses, including the horizontal responses and the vertical responses, between the asymmetrical suspended structure and the normal framed structure. As for the horizontal seismic responses in Figure 13a,b, it is interesting to note that the horizontal displacement and acceleration of the asymmetrical suspended structure were lower than those of the normal framed structure, which added columns below the suspended part. This result was mainly because the vertical vibration of the suspended part could consume the seismic energy, and the columns added below the suspended part constrained the vertical vibration. Based on the first passage failure criterion, it can be predicted that the asymmetrical suspension structure could achieve higher dynamic reliability of horizontal responses according to the smaller covariance of horizontal responses. In addition, the results of the vertical responses as shown in Figure 13c,d show that the vertical displacement and acceleration

of the asymmetrical suspended structure were larger than those of the normal framed structure, especially for the suspended part. It is predictable that the vertical displacement of the normal framed structure was close to zero, while the nodal vertical displacements of the suspended part were only near 1 mm, which is acceptable for practical engineering. However, the nodal vertical accelerations of the suspended part were two-times larger than the same part in the normal framed structure. The results also confirm these explanations for the smaller horizontal responses of the asymmetrical suspended structure, and they reveal that the vertical acceleration of the suspended part should raise concern.

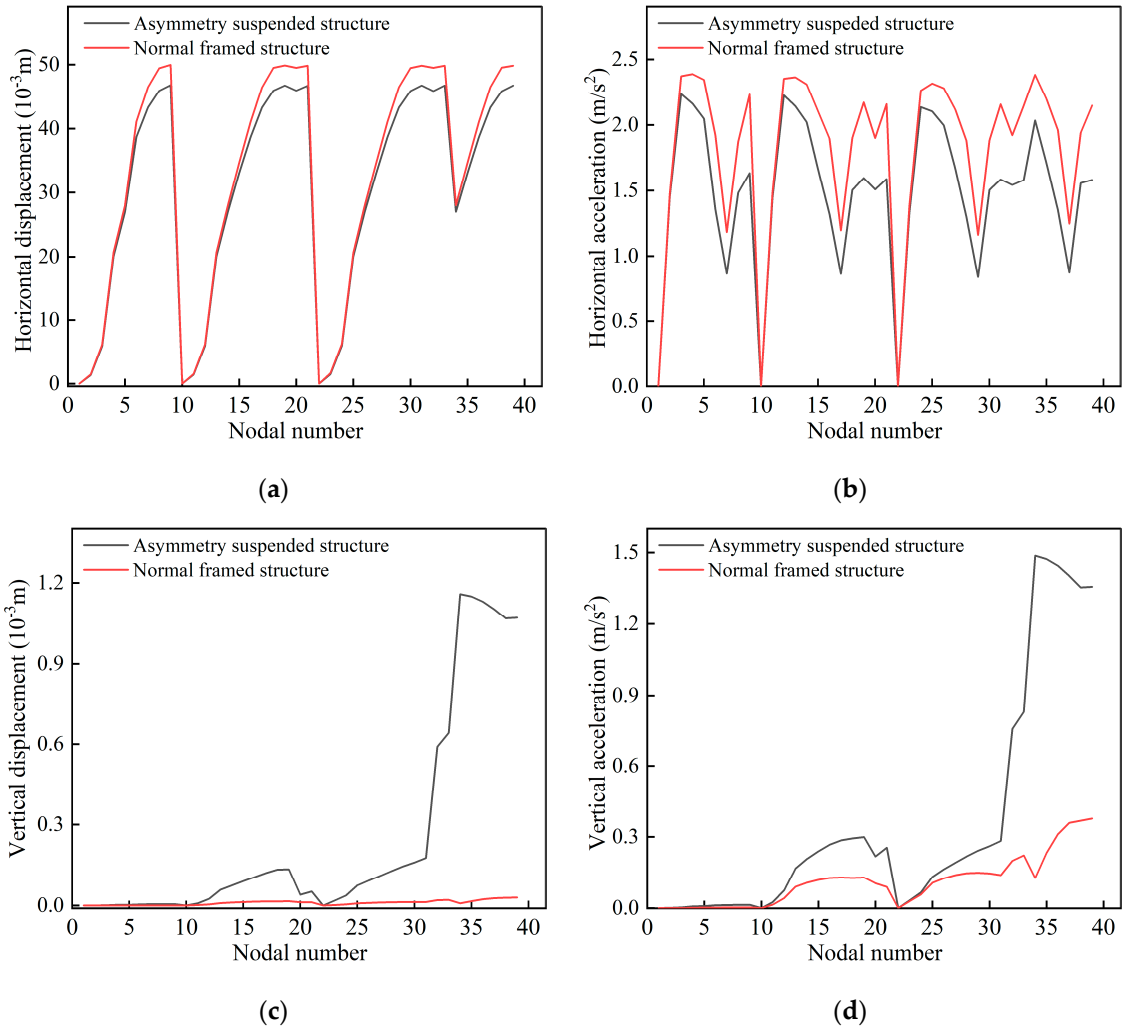


Figure 13. Comparison results of seismic responses between the asymmetrical suspended structure and the normal framed structure. (**a**) Horizontal displacement. (**b**) Horizontal acceleration. (**c**) Vertical displacement. (**d**) Vertical acceleration.

4.3. Comparison to the Symmetrical Suspension Structure

A comparative study on the asymmetrical and symmetrical suspension structures was also carried out to investigate the adaptability of the form of the suspended structure. Compared to the referenced asymmetrical suspended structure, the symmetrical suspended part was added to the symmetrical suspended structure, as shown in Figure 14. The nodal numbering was based on the asymmetrical suspended structure, the node number of the added suspended part followed the maximum value of the asymmetrical suspended structure, and the section properties of the added suspended part were the same as the symmetrical suspended part, as shown in Figure 14.

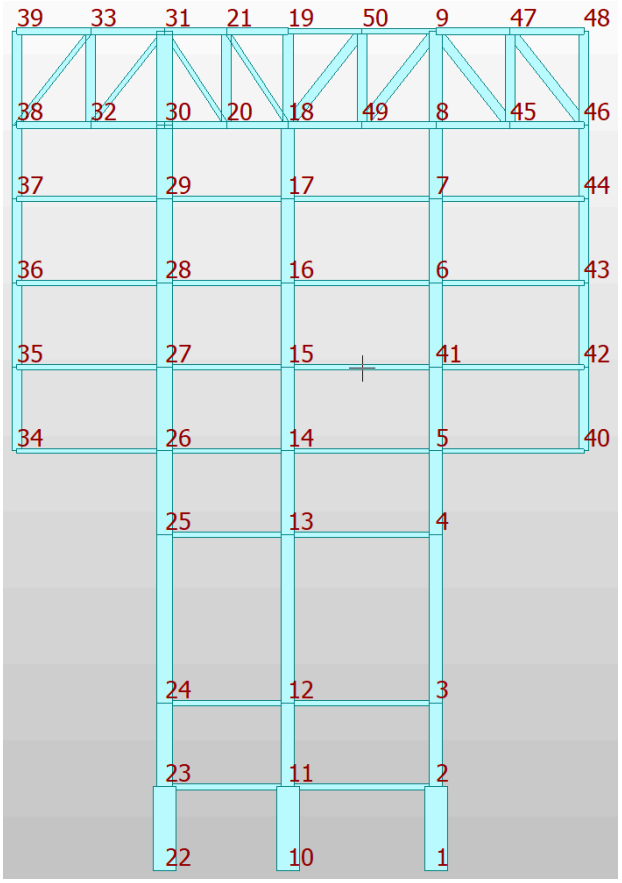


Figure 14. Schematic of the comparable symmetrical suspended structure.

The results of the seismic responses between the asymmetrical and symmetrical suspended structures were compared and are shown in Figure 15, including both the horizontal response and the vertical response. Compared to the asymmetrical suspended structure, the symmetrical suspended structure showed lower horizontal displacement and acceleration, as shown in Figure 15a,b. Two symmetrical suspended parts in the symmetrical suspended structure were more efficient in consuming the seismic energy than a single suspended part in the asymmetrical suspended structure. As for the vertical seismic responses, it can be observed that the vertical displacement and acceleration of the symmetrical suspended structure were larger than those of the asymmetrical suspended structure for almost all nodes, as shown in Figure 15c,d. Meanwhile, it can be seen that the nodes numbered 1–9 in the symmetrical suspended structure (near the suspended part) were larger than those in the asymmetrical suspended structure (away from the suspended part), which were close to zero. The nodes numbered 22–31 in both the asymmetrical and symmetrical suspended structure showed the same tendency as the nodes numbered 1–9 in the symmetrical suspended structure. In addition, the results indicate that the vertical responses of the columns near the suspended part were more remarkable than those further away from the suspended part. As a summary of the above discussion, the symmetrical suspended structure presented better anti-seismic behavior than the asymmetrical suspended structure from the aspect of both horizontal and vertical responses when subjected to horizontal seismic excitation.

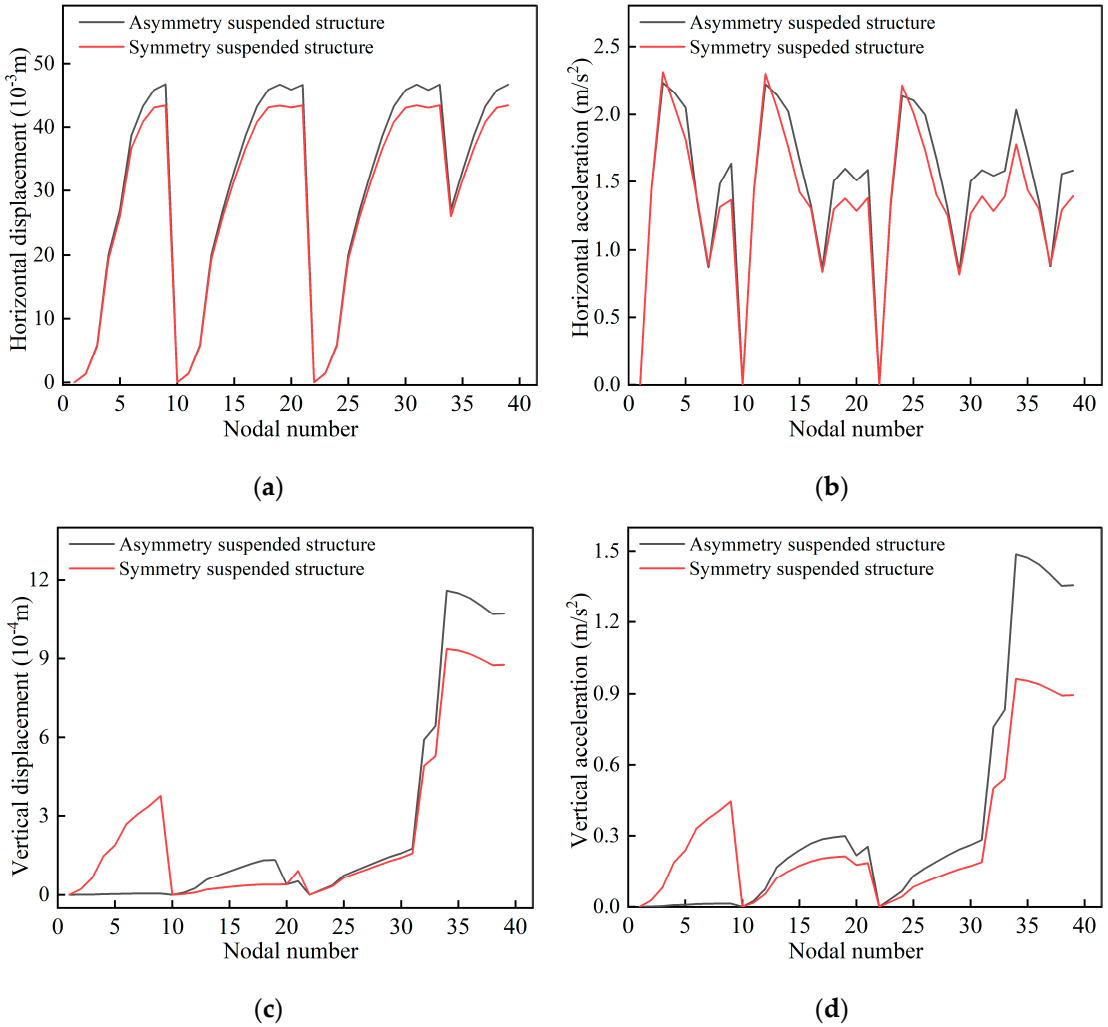


Figure 15. Comparison results of the seismic responses between the asymmetrical and symmetrical suspended structures. (**a**) Horizontal displacement. (**b**) Horizontal acceleration. (**c**) Vertical displacement. (**d**) Vertical acceleration.

5. Conclusions

An analytical study was conducted to investigate the dynamic responses of an asymmetrical suspended structure under random seismic excitation through creatively combining real model method decoupling, quadratic decomposition, and finite element modeling to obtain structural modal coefficients. The main conclusions are summarized below.

Through introducing the state variable and real mode transformation, the governing equation of the asymmetrical suspension structure was decoupled, and it was transferred into a linear combination of independent dynamic equations in generalized coordinates. Based on the frequency-domain solution of dynamic responses solved by the PEM, quadratic decomposition deduction was carried out on its PSDF. Subsequently, the closed-form solutions of the 0–2-order spectrum moments of dynamic responses were obtained based on the integration of the product of the 0–2-order power of frequency and the quadratic form of the PSDF. A practice case comparative study verified the superiority of the proposed method in terms of computational accuracy and efficiency in solving the random seismic responses of an asymmetrical suspended structure compared to the traditional PEM.

Extended analysis on various suspended spans and comparative studies on an asymmetrical suspended structure and a normal framed structure were also carried out. The results indicate that the horizontal displacement increased with the nodal height, and the

suspended part also followed the assumption of plane stiffness infinite under horizontal seismic excitation. It is interesting to find that the larger suspended span presented smaller horizontal displacement and acceleration due to the energy-consuming capacity of the suspended part. Compared to the normal framed structure, the asymmetrical suspended structure showed smaller horizontal responses and higher vertical responses, because the added columns supplied vertical support to constrain vertical movements, which limited the seismic energy dissipation of the original suspended part. Compared to the asymmetrical suspended structure, it can be seen that the symmetrical suspended structure presented lower horizontal and vertical responses, which was mainly because the two symmetrical suspended parts showed better seismic energy dissipation capacity than the single asymmetrical suspended part.

This paper innovatively derives the closed-form solution of dynamic responses of an asymmetrical suspension structure through creatively combining it with the finite element method for solving modal coefficients. In addition, the proposed method can be regarded as an instant calculating method with high accuracy, which abandons the larger number of iterations. However, only planar analysis was carried out in this work, and spatial analysis including the torsion effect are still limited, which could be the direction of further investigation.

Author Contributions: Methodology, M.C., X.L., Z.Y. and X.G.; Investigation and data curation, M.C. and X.G.; Writing, review and editing, X.G. and C.X.; Project administration, X.L., Z.Y. and X.G. All authors have read and agreed to the published version of the manuscript.

Funding: This research received no external funding.

Data Availability Statement: All the data are presented in the manuscript.

Conflicts of Interest: The authors declare no conflict of interest.

References

1. Lehmann, C.R. Multi-storey suspension structurcs. *Archit. Des.* **1963**, *11*, 530–565.
2. Ye, Z.; Feng, D.-C.; Wu, G. Seismic control of modularized suspended structures with optimal vertical distributions of the secondary structure parameters. *Eng. Struct.* **2019**, *183*, 160–179. [CrossRef]
3. Goodno, B.J.; Gere, J.M. Earthquake behavior of suspended-floor buildings. *J. Struct. Div.* **1976**, *102*, 973–992. [CrossRef]
4. Tu, Y.M.; Zhao, J.; Zhang, J.W.; Lv, Z.T.; China Civil Engineering Construction Corporation; Chinese Academy of Engineering; China Civil Engineering Corporation Limited; Tongji University; China Construction Engineering Co., Ltd (Eds.) Vibration Parameter Analysis of Suspended Building Structure. In Proceedings of the Shanghai International Conference on Technology of Architecture and Structure, Shanghai, China, 15–17 October 2009; Chinese Academy of Engineering, Civil, Hydraulic and Architecture Engineering Division: Beijing, China, 2019.
5. Shimanovsky, V.N.; Shimanovsky, A.V. Theory, calculation and design of space suspended roof systems for buildings. *J. Constr. Steel Res.* **1998**, *46*, 492–493. [CrossRef]
6. Liu, Y.; Lu, Z. Seismic Performance and Storey-Based Stability of Suspended Buildings. *Adv. Struct. Eng.* **2014**, *17*, 1531–1550. [CrossRef]
7. Saruta, M.; Wada, A.; Takeuchi, T.; Hikone, S.; Takahashi, T. Development of the core-suspended isolation system. *Earthq. Eng. Struct. Dyn.* **2011**, *40*, 429–447.
8. Nakamura, Y.; Okada, K. Effects and dynamic characteristics of the core-suspended isolation system assessed by long-term structural health monitoring. *Earthq. Eng. Struct. Dyn.* **2021**, *50*, 2259–2276. [CrossRef]
9. Zeng, B.; Gao, J.; Qing, Y.; Wang, C.-L.; Sun, X. Seismic performance of suspended-floor structures with viscous dampers considering acceptable interstory drift. *Struct. Des. Tall Spec. Build.* **2022**, *31*, e1912. [CrossRef]
10. Lv, Q.; Lu, Y.; Liu, Y. Vibration serviceability of suspended floor: Full-scale experimental study and assessment. *Structures* **2021**, *34*, 1651–1664. [CrossRef]
11. Zhao, X.; Wang, S.; Du, D.; Liu, W. Optimal Design of Viscoelastic Dampers in Frame Structures considering Soil-Structure Interaction Effect. *Shock Vib.* **2017**, *2017*. [CrossRef]
12. Paskalov, A.; Reese, S. Deterministic and probabilistic floor response spectra. *Soil Dyn. Earthq. Eng.* **2003**, *23*, 605–618. [CrossRef]
13. Chen, J.B.; Li, J. Optimal determination of frequencies in the spectral representation of stochastic processes. *Comput. Mech.* **2013**, *51*, 791–806. [CrossRef]
14. Conte, J.P.; Peng, B.F. Fully nonstationary analytical earthquake ground-motion model. *J. Eng. Mech.* **1997**, *123*, 15–24. [CrossRef]
15. Lin, Y.K.; Yong, Y. Evolutionary Kanai-Tajimi Type Earthquake Models. *J. Eng. Mech.* **1987**, *113*, 174–203. [CrossRef]
16. Kanai, K. An empirical formula for the spectrum of strong earthquake motions. *Bull. Earthq. Res. Inst. Univ. Tokyo* **1961**, *39*, 86–95.

17. Tajimi, H. A statistical method of determining the maximum response of a building structure during an earthquake. In Proceedings of the 2nd WCEE (Second World Conference on Earthquake Engneering), Tokyo, Japan, 11–18 July 1960; Volume 11, pp. 781–797.
18. Giaralis, A.; Taflanidis, A.A. Optimal tuned mass-damper-inerter (TMDI) design for seismically excited MDOF structures with model uncertainties based on reliability criteria. *Struct. Control. Health Monit.* **2018**, *25*, e2082. [CrossRef]
19. Calhoun, S.J.; Tehrani, M.H.; Harvey, P.S. On the performance of double rolling isolation systems. *J. Sound Vib.* **2019**, *449*, 330–348. [CrossRef]
20. Alotta, G.; Di Paola, M.; Pirrotta, A. Fractional Tajimi–Kanai model for simulating earthquake ground motion. *Bull. Earthq. Eng.* **2014**, *12*, 2495–2506. [CrossRef]
21. Bai, X.L.; Wu, Z.Y. Research on the parameter of response spectrum about Clough-Penzien model. In *Active and Passive Smart Structures and Integrated Systems 2011, Proceedings of the SPIE 2011, San Diego, CA, USA, 6–10 March 2011*; GhasemiNejhad, M.N., Ed.; SPIE: Bellingham, WA, USA, 2011; Volume 7977.
22. Lin, B.C.; Tadjbakhsh, I.G.; Papageorgiou, A.S.; Ahmadi, G. Response of base-isolated buildings to random excitations described by the Clough-Penzien spectral model. *Earthq. Eng. Struct. Dyn.* **1989**, *18*, 49–62. [CrossRef]
23. Cao, X.-Y.; Feng, D.-C.; Beer, M.J.S.S. Consistent seismic hazard and fragility analysis considering combined capacity-demand uncertainties via probability density evolution method. *Struct. Saf.* **2023**, *103*, 102330. [CrossRef]
24. Cao, X.-Y.; Feng, D.-C.; Li, Y. Assessment of various seismic fragility analysis approaches for structures excited by non-stationary stochastic ground motions. *Mech. Syst. Signal Process.* **2023**, *186*, 109838. [CrossRef]
25. Soong, T.T.; Grigoriu, M. *Random Vibration Mechanical and Structural Systems*; Prentice Hall: Englewood Cliffs, NJ, USA, 1993.
26. Clough, R.W.; Penzien, J. *Dynamics of Structures*, 2nd ed.; McGraw Hill: New York, NY, USA, 1993.
27. Ge, X.G.; Gong, J.H.; Zhao, C.J.; Azim, I.; Yang, X.; Li, C. Structural dynamic responses of building structures with non-viscous dampers under Kanai–Tajimi spectrum excitation. *J. Sound Vib.* **2021**, *517*, 116556. [CrossRef]
28. Liu, Q. Stationary random response of non-viscously damped polymer matrix composite structure systems. *Compos. Struct.* **2018**, *202*, 1–8. [CrossRef]
29. Lin, J.H.; Zhang, Y.H.; Zhao, Y. Pseudo excitation method and some recent developments. *Procedia Eng.* **2011**, *14*, 2453–2458. [CrossRef]
30. Ge, X.G.; Azim, I.; Li, C.D.; Gong, J.H.; Liu, M.; Zhao, C. Seismic responses of structure with six-element generalized model viscoelastic dampers. *Soil Dyn. Earthq. Eng.* **2023**, *164*, 107610. [CrossRef]
31. Ge, X.; Li, C.; Azim, I.; Gong, J.; Li, Y. Structural dynamic responses of linear structures subjected to Kanai-Tajimi excitation. *Structures* **2021**, *34*, 3958–3967. [CrossRef]
32. Yang, S.H.; Hsu, C.C.; Liang, J.J. Structural behavior of tall buildings with a new type of core-wall suspension structure. *J. Struct. Eng.* **2013**, *139*, 1210–1217.
33. Liu, Y.X.; Lu, Z.T. Seismic behavior of suspended building structures with semi-rigid connections. *Earthq. Struct.* **2014**, *7*, 415–448. [CrossRef]
34. Ye, Z.H.; Wu, G.; Feng, D.C.; Shafieezadeh, A. Shake table testing and computational investigation of the seismic performance of modularized suspended building systems. *Bull. Earthq. Eng.* **2020**, *18*, 5247–5279. [CrossRef]
35. He, Q.G.; Zhang, S.Q.; Shang, J.Y. Dynamic Characteristic and Parameter Analysis of a Modular Building with Suspended Floors. *Buildings* **2023**, *13*, 7. [CrossRef]

Disclaimer/Publisher's Note: The statements, opinions and data contained in all publications are solely those of the individual author(s) and contributor(s) and not of MDPI and/or the editor(s). MDPI and/or the editor(s) disclaim responsibility for any injury to people or property resulting from any ideas, methods, instructions or products referred to in the content.